Javier ARDUENGO[1*], Nicolas HASCOET[2]
Francisco CHINESTA[2], Jean-Yves HASCOET[1]

CLOSED-LOOP CONTROL OF EXTRUSION-BASED BIOPRINTING THROUGH REAL-TIME COMPUTER VISION

Bioprinting is the technology that combines the use of living matter and biomaterials to manufacture biological models, tissues, and structures layer by layer for applications in regenerative medicine, drug testing, and tissue engineering. Among bioprinting techniques, extrusion-based methods are the most widely used because of their relative simplicity, affordability, and ability to handle as wide range of biomaterials, including those with high viscosities. However, achieving consistent print quality remains a challenge, as the rheological properties of bioinks are highly variable and sensitive to environmental factors such as temperature. A critical aspect of print quality is maintaining a consistent and predictable line width, as pre-programmed trajectories and design fidelity rely on this parameter being well controlled. This work introduces a closed-loop control system for Extrusion-Based Bioprinting (EBB), utilizing real-time computer vision. The system employs a camera that is placed to monitor the line width immediately after extrusion, enabling real-time feedback to adjust the feedrate of the extrusion mechanism. This approach ensures consistent line widths across a wide range of materials and conditions, addressing the variability that traditionally hampers EBB. The method was validated using a Pluronic hydrogel, achieving closed-loop control over a wide range of target line widths. These findings demonstrate the potential for automated, robust bioprinting with improved reproducibility and precision, advancing the reliability of this technology for biomedical applications.

1. INTRODUCTION

Bioprinting, also referred to as Additive Biomanufacturing, is a revolutionary process combining biology and engineering to fabricate three-dimensional tissue-like structures. This is achieved by depositing bioinks layer by layer, often containing living cells, to replicate the architecture and functionality of natural tissues and organs. These bioinks are categorized into two types: cell-based bioinks, consisting solely of living cells, and hydrogel-based bioinks, which combine hydrogels with embedded cells. Applications of bioprinting span regenerative

_____

[1] Rapid Manufacturing Platform, Nantes Université, École Centrale Nantes, CNRS, GeM, UMR 6183, F-44000, France
[2] PIMM, Arts et Métiers Institute of Technology, CNRS-UMR 8006, F-75013, France
  E-mail: javier.arduengo-garcia@ec-nantes.fr, nicolas.hascoet@ensam.eu, francisco.chinesta@ensam.eu, jean-yves.hascoet@ec-nantes.fr
  https://doi.org/10.36897/jme/205422

medicine, where it is used to create tissue constructs for transplantation or to repair damaged organs; drug testing, providing highly accurate 3D tissue and organ models to test drug efficacy and safety; and biological research, enabling the study of disease mechanisms, tissue development, and cellular interactions in a controlled environment.

Bioprinting technologies are classified into three major approaches [1]:

- Extrusion-Based Bioprinting (EBB): This method uses syringe-like extruders to deposit bioink filaments through a nozzle. EBB accommodates a wide range of bioinks with high cell densities, making it ideal for complex tissue structures. Pneumatic systems are the most common due to their simplicity and sterile operation. However, precise geometric accuracy remains challenging due to the interplay of pressure, bioink flow, and filament shape (Fig. 1).

- Droplet-Based Bioprinting (DBB): Mimicking inkjet printers, DBB ejects bioink droplets using electrical, thermal, or acoustic energy. This technique excels in high-resolution printing, particularly for creating thin tissue layers and vascular networks, but is limited by the range of compatible bioinks.

- Light-Based Bioprinting (LBB): LBB utilizes laser energy for precise photopolymerization or bioink transfer, achieving high cell viability for intricate structures. However, its specialized bioinks and equipment can limit broader adoption.

Among these approaches, EBB is the most widely adopted due to its versatility and adaptability to various materials [2].
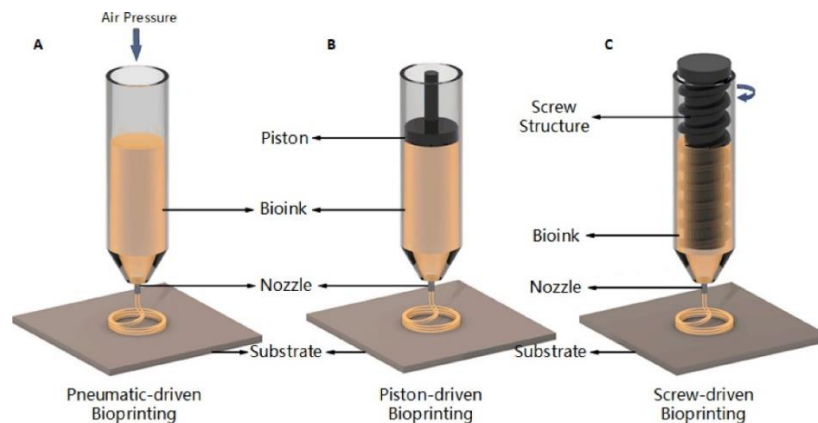

Fig. 1. Extrusion-based Bioprinting principal material actuation systems [3]

Overcoming challenges in EBB is pivotal for advancing its industrial and clinical applications. Key challenges involve managing filament shape during extrusion while balancing material properties, cell viability and printing parameters. Two critical dualities exemplify these challenges: (i) stiff hydrogels offer structural integrity but compromise cell viability, whereas softer hydrogels enhance viability at the cost of structural support; (ii) smaller needle diameters improve precision but increase shear stress, which reduces cell viability. Furthermore, spatial resolution, a fundamental factor, dictates deposition accuracy and influences both mechanical properties and the overall quality of bioprinted constructs [4].

Closed-loop control is crucial in EBB to address the variability in bioink composition and process complexity. Achieving consistent extrusion and deposition is hindered by bioink heterogeneity and environmental factors such as temperature fluctuations and dynamic flow. Open-loop systems, commonly used in current bioprinting hardware, lack real-time monitoring and adaptive control capabilities, leading to reduced fidelity in printed structures. Incorporating closed-loop systems ensures high fidelity in bioprinted constructs [5].

Innovations such as computer vision and Machine Learning (ML) offer promising solutions for real-time visual analysis and adaptive control. However, these advancements come with challenges, including higher computational requirements, resolution limitations, and environmental sensitivities [6].

This research addresses persistent challenges in EBB, particularly the inconsistencies in print quality due to the variability in bioink properties and environmental factors. While prior work has explored control and monitoring of output geometry, a need remains for a robust, adaptive system. To address this issue, this work introduces a closed-loop control system employing real-time computer vision.

2. ALGORITHM STATE OF THE ART

2.1. COMPUTER VISION FOR REAL-TIME APPLICATIONS

In the field of EBB, Computer Vision (CV) systems have become essential to enhance the manufacturing process through effective in situ monitoring. This technology enables continuous observation and analysis of the bioprinting environment, ensuring that production adheres to high standards of quality and precision.

Various specialized imaging sensors are used in these systems, each offering unique advantages and specific limitations that influence their application:

- Visible light cameras are relatively affordable and provide a wide field of view, allowing operators to monitor large areas. However, they are primarily limited to capturing two-dimensional surface information and have only modest resolution, which may not suffice for detailed assessments.
- Laser displacement scanners excel at creating accurate mapping of surface contours, but they may struggle with transparent materials, where laser beams may refract or scatter, leading to inaccurate measurements.
- Optical Coherence Tomography (OCT) can penetrate surfaces and identify internal defects, such as air bubbles or inconsistencies within the material. However, its high cost and narrow field of view can make widespread adoption in bioprinting applications challenging.

Recent advancements in bioprinting have underscored the significant role of integrated camera systems in monitoring extrusion processes and detecting anomalies in printed structures. The following topics group significant advancements in this field:

- Quality control and error mitigation: Armstrong et al. [7] employed integrated process monitoring and control strategies to measure feature errors in bioprinted

grids. This approach utilized optical images captured by a coaxial camera, which were subsequently processed to extract geometric data and derive defect patterns for monitoring. Moreover, the control strategy intelligently updated extrusion parameters in the G-code, enhancing accuracy in subsequent layers.

- Structural analysis and trajectory optimization: Gugliandolo et al. [8] demonstrated the effectiveness of optical imaging in bioprinting. By processing images from a coaxial camera, they identified structural defects and established a systematic approach for monitoring and control. This methodology not only led to improved anomaly detection but also provided insights into how extrusion parameters affect construct quality.
- Advanced monitoring techniques: Traditional camera systems often face limitations in resolution due to suboptimal positioning at large distances or oblique angles from the extrusion nozzle. Sergis et al. [9] addressed these challenges by designing a 3D bioprinting hardware prototype with an advanced camera system mounted on a transparent glass platform. This setup improves visibility and data capture, enabling high-resolution monitoring of bioink flow and filament formation. This innovation enhances the detection of structural anomalies and deepens understanding of how extrusion parameters influence construct quality.

2.2. CONTROL SYSTEMS AND ADDITIVE MANUFACTURING APPLICATIONS

Control theory is a multidisciplinary field that addresses the behaviour of dynamic systems and the design of mechanisms to regulate their behaviour to achieve desired outcomes. In the context of control systems, a fundamental distinction exists between open-loop control and closed-loop control [10]. Open-loop control systems operate without feedback. They execute a set of predefined actions without accounting for the current state of the system. While straightforward to implement and suitable for systems with predictable behaviour, they lack robustness against external disturbances or model inaccuracies. Closed-loop control systems, on the other hand, utilize feedback to continuously adjust the system's actions based on the difference between the desired and actual outcomes. This feedback mechanism, often implemented through algorithms like Proportional-Integral-Derivative (PID) control, enhances system stability and adaptability, making it indispensable in applications requiring precision.

Closed-loop control systems leverage a variety of advanced algorithms to maintain precision and adapt to dynamic conditions. Below is an overview of the major control strategies in additive manufacturing:

- Proportional-Integral-Derivative (PID) control: This widely used method maintains system stability by adjusting system parameters based on proportional, integral, and derivative terms of error magnitude. It is effective in applications such as temperature regulation, extrusion consistency, and motion control [11].
- Internal Model Control (IMC): It is a control strategy that incorporates an explicit model to predict system responses within the controller design. By leveraging the

internal model, IMC ensures better tracking of reference inputs in additive manufacturing, such as maintaining consistent filament geometry [12].

- Model Predictive Control (MPC): By leveraging a predictive model, MPC optimizes system behavior over a defined future horizon. It is highly effective in managing constrained systems, such as ensuring consistent extrusion while avoiding pressure or thermal limits [13].

2.2.1. CONTROL SYSTEMS IN ADDITIVE MANUFACTURING

These studies address challenges in extrusion closed-loop control within additive manufacturing, particularly for processes requiring high precision and adaptability:

- Liu et al. [14] proposed a closed-loop quality control system for fused filament fabrication that combines image-based defect detection with a tailored Proportional–Derivative (PD) control mechanism. Their system employs real-time image acquisition and classification to assess defect severity and adjust key process parameters.
- Tian et al. [15, 16] introduced a closed-loop strategy ensuring strand width uniformity using machine vision technology. A camera captures sequential strand images, which are processed to measure and adjust strand width in real time. Among the evaluated methods, the Smith PID controller delivered the most consistent results.
- Brion et al. [17] trained a neural network for real-time error detection and correction in diverse geometries and materials, integrating it with closed-loop control to optimize performance.
- Tamir et al. [18] used ML models with fuzzy logic to fine-tune 3D printing parameters, achieving improved structural properties through dynamic adjustments to extrusion and print speeds.
- Roach et al. [19] proposed a closed-loop system combining Invertible Neural Networks (INNs) and in situ vision for defect detection and rapid correction of extrusion parameters.
- Ma et al. [20] developed a monitoring system for silicone additive manufacturing using a laser sensor for iterative optimization. Although effective for substrate-bound strands, spatial strand optimization remains an area for future improvement.

2.3. CONTROL SYSTEMS FOR EXTRUSION-BASED BIOPRINTING

Extrusion-Based Bioprinting Process Model

The mathematical expression of the physical model for the extrusion-based bioprinting process is presented in Eq. 1 [21]:

$$2R_p = w = D^2 \sqrt{\frac{1}{332 \cdot \eta \cdot L \cdot v_p} \cdot \left(\frac{4n}{3n} + 1\right) \cdot \Delta P} \tag{1}$$

Where w is the line width, ΔP is the extrusion pressure v_p is the printing feedrate, L is the length of the nozzle, D is the diameter or size of the nozzle, and η is the apparent viscosity.

Derived from this equation, two main mechanisms to control the output geometry can be identified: (i) through extrusion pressure and (ii) through feedrate. Furthermore, it can be deduced that the relation between width and pressure or feedrate is non-linear. This section presents an overview of recently proposed control systems designed for EBB.

Open-Loop Control Systems

As previously discussed, open-loop control systems are straightforward and rely on predefined inputs without incorporating feedback. In bioprinting setups, this simplicity makes them widely used. Several recent studies highlight the application of open-loop control in optimizing parameters and improving outcomes in EBB: Trucco et al. [21] utilized an analytical model based on hydrogel rheology to predict filament width, achieving enhanced printing accuracy through a power-law model validated experimentally. Arjoca et al. [22] employed statistical regression to optimize extrusion speed and predict filament diameter using non-Newtonian hydrodynamic principles. Arduengo et al. [23] combined ML with automated image analysis to guide parameter selection, demonstrating the potential of open-loop systems.

Closed-Loop Control Systems

The implementation of fully integrated closed-loop control systems in EBB remains limited. However, recent advancements in extrusion-based additive manufacturing provide promising insights into the potential applications of such systems for bioprinting [24]. Recent works have explored closed-loop approaches: Wenger et al. [25] developed a PID-based closed-loop control system for pneumatic extrusion. The system integrates a flow sensor to measure ink flow in real time, dynamically adjusting extrusion pressure. This method maintains consistent flow rates that adjust to varying conditions. Kelly et al. [26] recently introduced an Artificial Intelligence (AI) driven closed-loop bioprinting platform designed for real-time quality assessment and error correction. A custom bioprinter equipped with an integrated camera leverages convolutional neural networks to classify extrusion quality in various printing scenarios. Using real and synthetic training data, the system dynamically adjusts extrusion parameters to address errors, achieving correction of over- and under-extrusion issues in bioinks like alginate and collagen.

3. MATERIALS AND METHODS

This section provides a comprehensive description of the bioprinting setup, experimental protocol, and software framework used to achieve precise material extrusion. It outlines the components of the custom-built bioprinter, the methodologies employed to ensure consistent performance, and the algorithms driving the feedback loop and tuning for optimal operation.

3.1. SETUP AND MATERIALS

The bioprinting setup is a custom prototype built for precise material extrusion, featuring centralized electronic control for seamless integration of components. Key components include (Fig. 2):
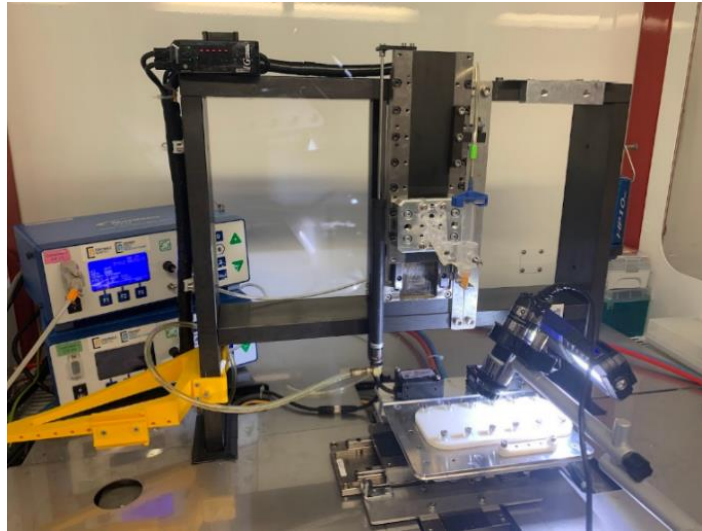

Fig. 2. Image of the experimental setup shows the bioprinting stage at the center, with the syringe mounted on the printhead and the camera pointing to the printing zone. The printing substrate is fixed to the buildplate, and additional lighting ensures clear image capture

- Bioprinter stage: The bioprinter is a Cartesian machine built in-house, featuring buildplate movement driven by Parker MX80LS linear motors. These motors enable 140mm *XY* travel with 0.1 μm encoder resolution and ±3 μm of positional accuracy. The Z-axis controls the syringe vertically, while an MC405 motion controller (Trio Motion Technology) with an ARM11 processor manages all axes.
- Pressure controller: Pneumatic control within the syringe is handled by a Nordson Ultimus V pressure controller, offering a resolution of 1 mbar, ±140 mbar accuracy a maximum pressure of 5 bar. This system supports electronic control of dispense time and pressure settings via a serial interface.
- Printing area: The bioprinter operates in a microbiological safety hood, which minimizes contamination risks. The printing area includes a substrate fixed to the buildplate and a calibration reference fabricated using Rigid 10K Resin with a Formlabs Form 3+ Stereolitography (SLA) 3D printer.
- Bioink: The hydrogel material used is Pluronic F-127 (Merck, P2443-250G), chosen for its temperature-sensitive properties. It is prepared by dissolving the polymer at a 25% w/v concentration in deionized water at 4 °C. Blue food coloring is added for improved visibility, and air bubbles are removed through centrifugation. Although non-cell-laden bioinks are used here, the system is compatible with living cell-laden formulations.
- Syringe and needle: Bioink is extruded using a 3cc syringe (Nordson, P/N: 7366044) connected to the pressure controller via an adapter (Nordson, P/N: 7012341). The

stainless steel needle used has an inner diameter of 0.41 mm, an outer diameter of 0.72 mm, and a length of 38.1 mm (Nordson, P/N: 7018266).

- Camera: A Dino-Lite microscopic camera (P/N: AM7915MZTL) is mounted to monitor the needle's movement and material deposition. Its alignment ensures detailed visualization of the filament during extrusion. Used at a resolution of 1280 x 960 pixels per frame, representing 6.5 µm per pixel at the applied field of view.
- PC: All electronic components, including the bioprinter stage, the pressure controller and the camera are controlled by a C++ program running on a PC (12th Gen Intel Core i5-12500H and 16 GB RAM), which hosts all real-time processing. Interface with the bioprinter stage is ensured through an ethernet connection and the C++ API provided by the manufacturer [27]. The camera is connected through USB and controlled using the open-source library OpenCV [28], which was also used for image treatment in the developed computer vision algorithm. The pressure controller is connected to the PC through a Serial-to-USB adapter, and code was written to communicate based on the manufacturer's serial protocol [29].

3.2 EXPERIMENTAL PROTOCOL AND SOFTWARE

The experimental protocol and software are integral to maintaining precise control of the printed line width through an automated feedback loop. The setup operates as follows:

1. Parameter setup: Several parameters are set manually, including the pneumatic pressure, printing height, and an initial feedrate. The target width is defined as a function of time or distance and preloaded into the control software.
2. Material purging: Material purging ensures consistent material flow by eliminating air bubbles and blockages, reducing inconsistencies in the extrusion process.
3. Calibration: A calibration phase uses a reference dot with a known size placed under the camera. The software calculates the scale for converting pixel dimensions to millimeters, ensuring accurate width measurements.
4. Positioning and extrusion start: The needle is positioned at the starting point of the substrate, and extrusion begins. Once the camera captures a stable reading of the line width, the feedback control loop is activated, dynamically adjusting the feedrate to maintain the desired line width.
5. Feedback loop: During operation, the program processes each frame captured by the camera to measure the extruded line's width. An IMC controller dynamically adjusts the printer's feedrate based on these measurements to maintain the target width, while validation filters out erratic measurements.
6. Data logging and monitoring: The program logs critical data, including timestamps, measured and targeted width and feedrate, exporting them into a file for analysis.
7. End condition: When the needle reaches the end of the substrate, the extrusion and movement stop, completing the printing cycle.

The software (a C++ program) is hosted on the PC and orchestrates the entire process. It manages both the preparation steps and the real-time processing pipeline, which includes frame acquisition from the camera, execution of the computer vision algorithm, and

computation of the response according to the selected control architecture (open-loop or closed-loop). The program then communicates the updated speed to the bioprinting stage for immediate application. The software runs a single-loop structure, ensuring efficient and consistent operation during the feedback control phase. The effective sampling frequency was 9.0 Hz, with an accuracy of ±2.8 Hz at 95% confidence, based on variation in elapsed time under stable conditions. This frequency is limited mostly by the camera latency (~105 ms) to retrieve each frame.

<p style="text-align:center">3.3 CONTROLLER DESIGN</p>

The controller uses an IMC architecture hosted inside the C++ program (digital implementation), with a model that predicts output feedrate based on input target width. The output feedrate is the sum of this prediction and a Proportional-Integral response which ensures convergence of target and measured width (Eq. 2):

$$v_p(t) = v_{pred}\big(w_c(t)\big) + K_p(t) \cdot e(t) + K_i(t) \int e(t)\, dt, \qquad e(t) = w_c(t) - w(t) \qquad (2)$$

where $w_c(t), w(t)$ are the target and measured width at time t, $v_{pred}\big(w_c(t)\big)$ is the feedrate predicted by the internal model based on the target width, $v_p(t)$ is the output feedrate, $e(t)$ is the error and $K_p(t), K_i(t)$ are the proportional and integral gains, respectively. They are computed as a function of the system's sensitivity to maximize time responsiveness without leading to instabilities for every target width, given the non-linearity of the system.

Feedrate Prediction Internal Model

The internal model predicts feedrate based on target width. It is computed interpolating five points (feedrate vs. width) measured in a calibration pass. The obtained curve depends on the material rheological properties and the extrusion pressure.

Gain Scheduling

The gain of the controller is adjusted depending on the system's sensitivity at each operational point. The slope of the internal model is used as a prediction of the sensitivity (Eq. 3):

$$K_i(t) = k \cdot \frac{d}{dw_c} v_{pred}\big(w_c(t)\big), \quad K_p(t) = K_i(t) \cdot 0.1 \qquad (3)$$

K_i being proportional to the sensitivity by a constant k and K_i and K_p keeping a constant ratio of 10 to 1.

Validation Criteria

Before applying the computed response, the controller validates measurements to filter out anomalies from air bubbles or extrusion discontinuities. The algorithm ensures spatial coherence by analyzing boundary positions identified through computer vision. Significant deviations invalidate the measurement, leveraging the detection algorithm's stochastic outputs when no line is present. If validation fails, the controller maintains its current state to prevent erroneous corrections.

3.4. OPEN-LOOP MACHINE LEARNING BASED CONTROL SYSTEM

Along with this IMC closed-loop system, a novel open-loop ML based approach has also been tested for comparison. Based on a beforehand training in an open-loop context [23], a width manifold is created (Fig. 3).

The intersection between a hyperplane and the manifold represents the possible parameters sets meeting the target width. The remaining choices can then be sorted based on the repeatability and quality metrics proposed in [23]. Training the ML model can be time consuming, but the prediction is done in real-time (0.5 ms on average over 10k runs). The inverse model prescribing the process parameters is an optimization problem on the manifold built in the previous step for a given target width.
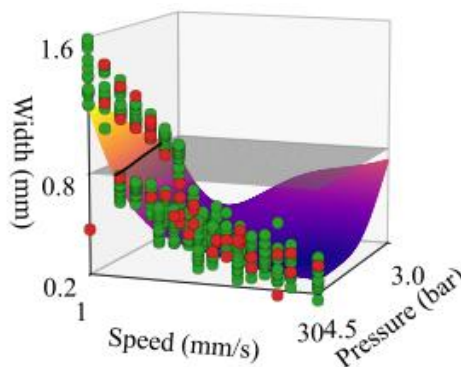

Fig. 3. Width manifold in function of the speed and pressure. Green points are the data used for training the ML model where red points are for validating the model. The gray hyperplane is an example of a 0.8 mm target width where the intersection with the manifold corresponds to the possible process parameters meeting this target

For a given target width, the model can propose a set of process parameters within 6 ms on average (over 10k runs for different target width from 0.16 mm to 1.59 mm).

3.5. COMPUTER VISION ALGORITHM

The algorithm analyzes a strip of the camera's captured frame to identify the printed line's width through (Fig. 4):

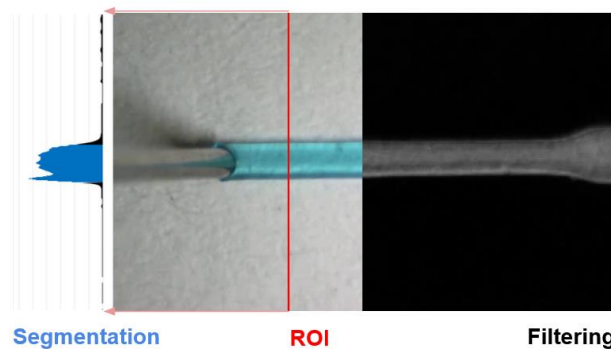**Segmentation**   **ROI**   **Filtering**

Fig. 4. Frame showing the selected ROI and the obtained clustering of the pixels after black and white conversion

- Profile reduction: Reduces the Region Of Interest (ROI) into a 1D intensity profile by averaging pixel values across rows.
- Black and white filtering: Combines the saturation channel with the inverted red channel to isolate the line's contour. The resulting profile is smoothed to reduce noise.
- K-means clustering segmentation: Segments the smoothed profile into foreground and background regions, identifying the largest contiguous region as the line width.

The accuracy of the computer vision system was evaluated to be ±21 µm at 95% confidence (standard deviation of around 10 µm), based on the analysis of noise when measuring a constant width.

4. RESULTS

Frequency response of the extrusion system

The system was fed with oscillatory input (feedrate, centred at 5 mm/s with 3 mm/s amplitude), and the output oscillations (width) were analysed using FFT analysis for amplitude gain and phase shift. This allowed for the empirical construction of the system's Bode diagram, which clarifies its behaviour and characteristics (Fig. 5):
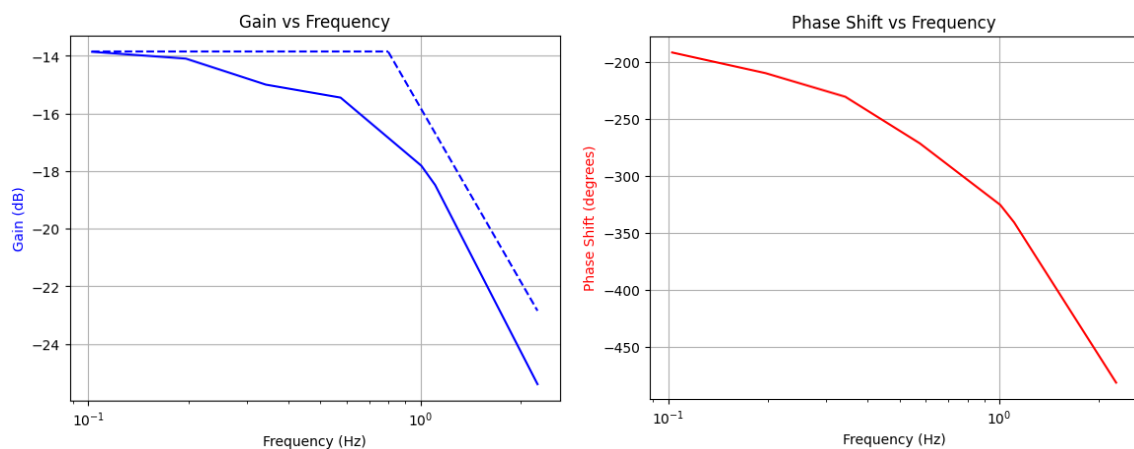

Fig. 5. Bode diagram of the extrusion system. On the left, gain as a function of frequency. Estimated asymptotic trend is showed as a dotted line with a slope of –20 dB/decade, hinting a behaviour of a first-order low-pass filter with a cut-off frequency of 0.8 Hz. On the right, phase shift as a function of frequency, asymptotic to the left at –180° as the relation between feedrate and width is inverse, and decaying, hinting that the system presents lag, estimated at 0.37 seconds

The given Bode diagram suggests that the system behaves as a first-order low-pass system with a constant time delay. This conclusion is based on the following observations:

- The gain plot exhibits a nearly constant value at low frequencies (–14 dB), followed by a roll-off at higher frequencies. The roll-off slope is -20 dB/decade, which is characteristic of a single-pole system. The cut-off frequency, defined by the -3 dB drop from the low-frequency gain, is estimated at 0.8 Hz, indicating the dominant pole location.

- The phase plot shows a linear decrease with frequency, which is a strong indicator of a constant time delay in the system. The estimated slope suggests a time delay of 0.37 ± 0.01 seconds (95% confidence using the Cramér–Rao lower bound for phase estimation in Gaussian noise). Also, the phase shift asymptotic to the left seems to be –180°. This is due to the inverse relation between feedrate and width.

Step response of the controlled extrusion system

The step response of the system was assessed through a series of incremental reductions in the target width. The initial target width was set to 1.5 mm, followed by successive decreases, with each step allowing for the measurement of the convergence time. This convergence time is defined as the interval between the application of a new target width and the moment when the measured width stabilizes within a 5% tolerance range of the target, as depicted by the blue shaded regions in (Fig. 6). At least three tests were carried out for each target width, representing here the most significant one (i.e. highest response time).

The results indicate that the system effectively reaches all target widths within the range of [0.4, 1.5] mm between 0.9 ± 0.1 and 1.6 ± 0.1 seconds (accuracy based on the system's sampling frequency). The predicted feedrates derived from the internal model do not immediately yield the desired width, as evidenced by the initial decrease in width, which is highlighted by the red curves in Fig. 6 showing transient response and overshoot. Nevertheless, the integral control actions facilitate convergence thereafter. In convergence, the width was found to vary with a mean standard deviation of 16 μm, increasing at a mean rate of 18 μm per mm in target width as the system becomes more sensitive to changes in speed.
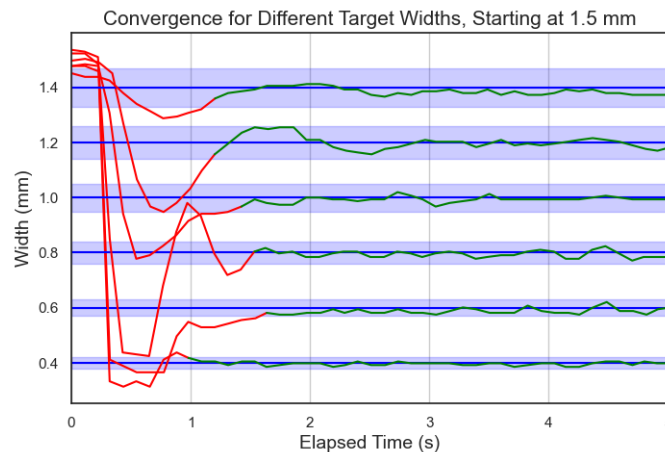

Fig. 6. Evolution in time of the width (red/green) when applying a step in the target width (blue, 5% tolerance band in shaded blue). The signal turns green once it enters the convergence band, showing a convergence time ranging between 0.9 and 1.6 seconds. Negative initial overshoot is mainly due to internal model inaccuracies and lag

On the other hand, the open-loop ML based approach does not show any width oscillation. The predicted speed for a new target width is applied instantaneously and seen in the following cycle of the control system. This approach, based on a data-driven inverse model, directly proposes an optimal set of process parameters for a target width. The response

time for any width change is therefore the same and depends only on the optimization process when querying the manifold.

5. CONCLUSION

This paper introduces a novel approach for a closed-loop control system for EBB that integrates real-time computer vision with an IMC controller to ensure a consistent and robust output width, along with an open-loop ML based system which ensures an instantaneous and well-tuned response. The system operates at a high sampling rate of approximately 9.0 Hz, achieving an error of less than 5% within 2 seconds for the closed-loop approach. Its flexibility, accommodating widths from 0.4 mm to 1.5 mm, ensures stability across the entire range despite the inherent non-linearity of the process. This demonstrates significant improvements in responsiveness with respect to previous studies, as those presented by Tian et al. [15, 16] and Brion et al. [17]. Given the susceptibility of EBB to perturbations (knowing that error accumulates layer by layer), this closed-loop approach significantly outperforms open-loop systems, as demonstrated in Fig. 7.
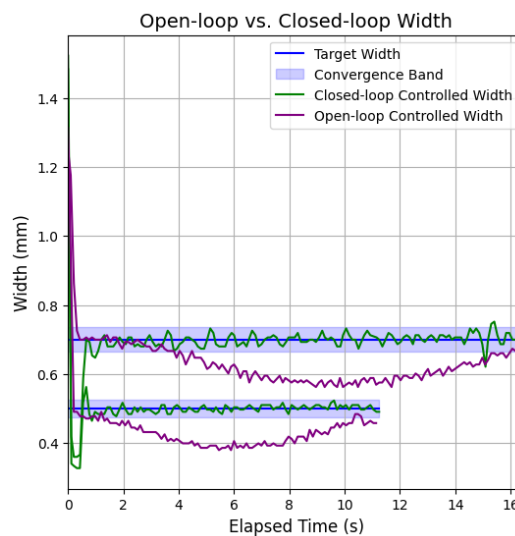

Fig. 7. Comparison of closed-loop control vs open-loop control. The open-loop system is subject to variations in the printing height due to substrate wrapping, which is a position-dependant perturbation, consistent through the presented tests. The closed-loop system is able to correct for this perturbation

The open-loop ML approach clearly improves the system responsiveness, providing an instantaneous direct response, but lacks resilience to unknown perturbation, noise or any event not planned during the training phase of the model. Therefore, future work will focus in implementing the ML based model as an internal model for IMC, thus providing a quick response without oscillation as well as robustness against perturbations.

Designed to meet the stringent requirements of bioprinting, the system ensures non-contact operation and maintains sterility, making it well-suited for biomedical applications. Furthermore, the methodology presented in this work is highly adaptable and can be extended

to other additive manufacturing techniques that demand precise material deposition and real-time process control.

Applied currently to single-strand Pluronic extrusion, future work will explore its extension to multilayer constructs, cell-laden bioinks, and a broader range of printable materials, with the aim of validating performance under more complex and biologically representative printing conditions.

REFERENCES

[1]   IBRAHIM T. OBZOLAT., 2017, *3D Bioprinting - Fundamentals, Principles and Applications*, Elsevier Inc.

[2]   LIU C., LIU J., YANG C., TANG Y., LIN Z., LI L., LIANG H., LU W., WANG L., 2022, *Computer Vision-Aided 2D Error Assessment and Correction for Helix Bioprinting*, International Journal of Bioprinting, 8/2, 547, https://doi.org/10.18063/ijb.v8i2.547.

[3]   GU Z., FU J., LIN H., HE Y., 2020, *Development of 3D Bioprinting: from Printing Methods to Biomedical Applications*, Asian Journal of Pharmaceutical Sciences, 15/5, 529–557, https://doi.org/10.1016/j.ajps.2019.11.003.

[4]   HINTON T.J., LEE A., FEINBERG A.W., 2017, *3D Bioprinting from the Micrometer to Millimeter Length Scales: Size Does Matter*, Current Opinion in Biomedical Engineering, 1, 31–37, https://doi.org/10.1016/j.cobme.2017.02.004.

[5]   DABABNEH A., OZBOLAT I., 2014, *Bioprinting technology: A Current State-of-the-Art Review*, Journal of Manufacturing Science and Engineering, 136/6, 061016, https://doi.org/10.1115/1.4028512.

[6]   BARJUEI E.S., SHIN J., KIM K., LEE J.., 2024, *Precision Improvement of Robotic Bioprinting via Vision-Based Tool Path Compensation,* Scientific Reports, 14, 17764.

[7]   ARMSTRONG A., PFEIL A., ALLEYNE A., JOHNSON A.W., 2021, *Process Monitoring and Control Strategies in Extrusion-Based Bioprinting to Fabricate Spatially Graded Structures*, Bioprinting, 21, https://doi.org/10.1016/j.bprint.2020.e00126.

[8]   GUGLIANDOLO S.G., MARGARITA A., SANTONI S., MOSCATELLI D., COLOSIMO B.M., 2022, *In-Situ Monitoring of Defects in Extrusion-Based Bioprinting Processes Using Visible Light Imaging,* V CIRP Conference on BioManufacturing, 110, 219–224, https://doi.org/10.1016/j.procir.2022.06.040.

[9]   SERGIS V., KELLY D., BRITCHFIELD G., PRAMANICK A., MASON K., DALY A., 2025, *In-Situ Quality Monitoring During Embedded Bioprinting Using Integrated Microscopy and Classical Computer Vision*, Biofabrication, 17/2, https://doi.org/10.1088/1758-5090/adaa22.

[10]   ASTRÖM K.J., MURRAY R., 2008, *Feedback Systems: An Introduction for Scientists and Engineers,* DRAFT v2.4a, © 2006 Karl Johan ˚Astr¨om and Richard Murray.

[11]   MATAMOROS M., GOMEZ-BLANCO J.C., SANCHEZ J.A., MANCHA E., MACROS A.C., CARRASCO-AMADOR P., PAGADOR J.B., 2020, *Temperature and Humidity PID Controller for a Bioprinter Atmospheric Enclosure System*, Micro-machines, 11, 999, https://doi.org/10.3390/mi11110999.

[12]   ROJAS C.J.G., PORTILLA C., ÔZKAN L., 2024, *Model-Based Feedback Control of Filament Geometry in Extrusion-Based Additive Manufacturing*, IFAC Papers OnLine, 58, 403–408, 12th IFAC Symposium on Advanced Control of Chemical Processes (ADCHEM), https://doi.org/10.1016/j.ifacol.2024.08.370.

[13]   ZOMORODI H., LANDERS R., 2016, *Extrusion Based Additive Manufacturing Using Explicit Model Predictive Control*, American Control Conference (ACC), 1747–1752, IEEE, Boston, MA, USA.

[14]   LIU C., LAW A.C.C., ROBERSON D., KONG Z., 2019, *Image Analysis-Based Closed Loop Quality Control for Additive Manufacturing with Fused Filament Fabrication,* Journal of Manufacturing Systems, 51, 75–86, https://doi.org/10.1016/j.jmsy.2019.04.002.

[15]   TIAN X., LI Y., MA D., HAN J., XIA L., 2021, *Closed-Loop Control of Silicone Extrusion-Based Additive Manufacturing Based on Machine Vision,* International Manufacturing Science and Engineering Conference, https://doi.org/10.1115/MSEC2021-63719.

[16]   TIAN X., LI Y., MA D., HAN J., XIA L., 2022, *Strand Width Uniformly Control for Silicone Extrusion Additive Manufacturing Based on Image Processing*, International Journal of Advanced Manufacturing Technology, 119, 3077–3090.

[17]   BRION D., PATTINSON S., 2022, *Generalisable 3D Printing Error Detection and Correction Via Multi-Head Neural Networks*, Nature Communications, 13, 4654.

[18] TAMIR T., XIONG G., FANG Q., YANG Y., SHEN Z., ZHOU M., JIANG J., 2023, *Machine-Learning-Based Monitoring and Optimization of Processing Parameters In 3D Printing*, International Journal of Computer Integrated Manufacturing, 36/9, 1362–1378, https://doi.org/10.1080/0951192X.2022.2145019.

[19] ROACH D.J., ROHSKOPF A., LEGUIZAMON S., APPELHANS L., COOK A.W., 2023, *Invertible Neural Networks for Real-Time Control of Extrusion Additive Manufacturing*, Additive Manufacturing, 74, 103742, https://doi.org/10.1016/j.addma.2023.103742.

[20] MA D., TIAN X., CHANG T., HUSSAIN S., XIA L., HAN J., 2024, *In-Situ Process Monitoring and Optimization for Extrusion-Based Silicone Additive Manufacturing*, 19th International Manufacturing Science and Engineering Conference (MSEC), Knoxville, Tennessee, USA, https://doi.org/10.1115/MSEC2024-130739.

[21] TRUCCO D., SHARMA A., MANFERDINI C., GABUSI E., PETRETTA M., DESANDO G., RICOTTI L., CHAKRABORTY J., GHOSH S., LISIGNOLI G., 2021, *Modeling and Fabrication of Silk Fibroin–Gelatin-Based Constructs Using Extrusion-Based Three-Dimensional Bioprinting*, ACS Biomaterials Science and Engineering, 7/7, 3306–3320, https://doi.org/10.1021/acsbiomaterials.1c00410.

[22] ARJOCA S., BOJIN F., NEAGU M., PˇAUNESCU A., NEAGU A., PAUNESCU V., 2024, *Hydrogel Extrusion Speed Measurements for the Optimization of Bioprinting Parameter*s, Gels, https://doi.org/10/2, 10.3390/gels10020103.

[23] ARDUENGO J., HASCOËT N., CHINESTA F., HASCOËT J-Y., 2024, *Open-Loop Control System for High Precision Extrusion-Based Bioprinting Through Machine Learning Modeling*, Journal of Machine Engineering, 24/1, 103–117, https://doi.org/10.36897/jme/186044.

[24] SINGH M., 2021, *Sensor-Based Characterization and Control of Additive Biomanufacturing Processes*, PhD thesis, Virginia Tech.

[25] WENGER L., STRAUß S., HUBBUCH J., 2022, *Automated and Dynamic Extrusion Pressure Adjustment Based on Real-Time Flow Rate Measurements for Precise Ink Dispensing in 3D Bioprintin*g, Bioprinting, 28, https://doi.org/10.1016/j.bprint.2022.e00229.

[26] KELLY D., SERGIS V., VENTURA-BLANCO L., MASON K., DALY A.C., 2024, *Autonomous Control of Extrusion Bioprinting Using Convolutional Neural Networks*, Advanced Functional Materials, 2424553, https://doi.org/10.1101/2024.12.07.627315.

[27] Trio Motion Technology, 2025, *Software Downloads and Support*, Available at: www.triomotion.com/public/software/ softwareSupport.php (Accessed: 4 May 2025).

[28] BRADSKI G., 2000, *Dr.Dobb's, Journal of Software Tools,* The OpenCV Library.

[29] Nordson EFD, Ultimus V High Precision Dispenser, Available at: https://www.nordson.com/en/products/efd-products/ultimus-v-dispensers (Accessed: 4 May 2025).